Volume 52
Number 16
28 April 2023
Pages 4987-5384

Dalton Transactions

An international journal of inorganic chemistry

rsc.li/dalton

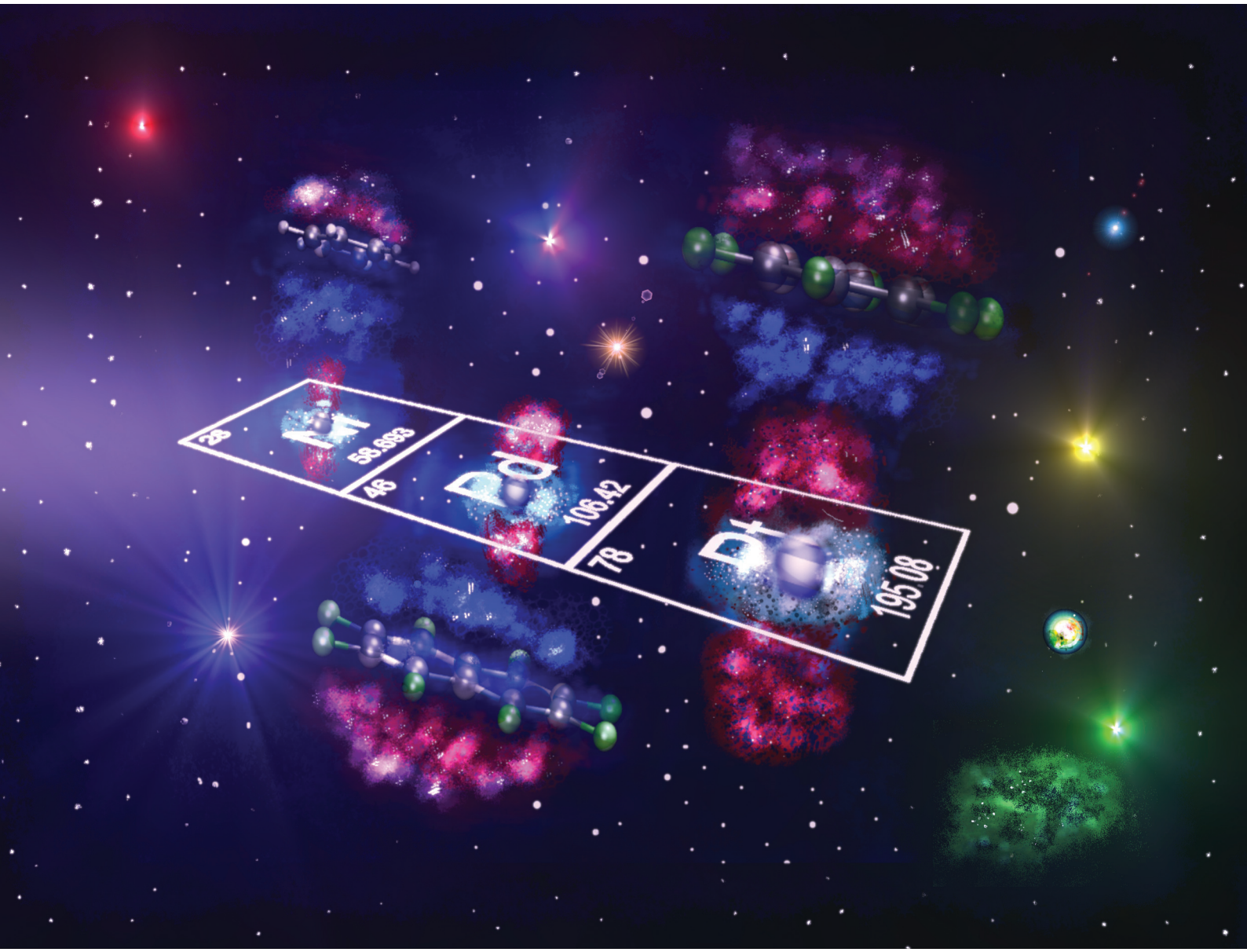

ISSN 1477-9226

ROYAL SOCIETY OF CHEMISTRY

PAPER

Giuseppe Resnati, Antonio Frontera *et al.*

Group-10 π-hole···d_{z^2}[M^{II}] interactions: a theoretical study of model systems inspired by CSD structures

Dalton Transactions

ROYAL SOCIETY OF CHEMISTRY

PAPER

View Article Online
View Journal | View Issue

Cite this: *Dalton Trans.*, 2023, **52**, 5056

Group-10 π-hole···d_{z^2}[M^{II}] interactions: a theoretical study of model systems inspired by CSD structures†

Miriam Calabrese, [a] Sergi Burguera, [b] Giuseppe Resnati *[a] and Antonio Frontera *[b]

In recent years Pd(II) and Pt(II) cases have been reported wherein metals in square planar complexes were used as nucleophilic partners to construct supramolecular assemblies with electrophilic molecules like σ-hole and π-hole donors. The formation of such assemblies is based on the nucleophilicity and accessibility of the d_{z^2} orbital (in group-10 elements) in the square-planar complexes. This opens new avenues in inorganic chemistry and crystal engineering as it enriches the current toolbox of noncovalent interactions and supramolecular synthons thus allowing the design of new types of architectures in the solid state. This manuscript reports a comprehensive theoretical study characterizing π-hole···d_{z^2}[M^{II}] (M = group 10 element) interactions from an energetic point of view. Several computational tools based on the topology of the electron density are used. Examined systems had been identified by considering structures in the Cambridge Structural Database where this interaction was used to construct supramolecular assemblies. Several aromatic rings have been used, varying from π-basic to π-acid rings by adjusting the number of fluorine substituents. Moreover, the influence of metal···metal interactions on the nucleophilicity of the d_{z^2} orbital has been studied using MEP surface analysis. The π-hole energies are moderately strong (from −5 to −10 kcal mol^{-1}) and the crucial role of dispersion forces is revealed.

Received 7th March 2023,
Accepted 28th March 2023

DOI: 10.1039/d3dt00698k

rsc.li/dalton

Introduction

Most common lone pair (lp) bearing atoms are the lighter elements of groups 15–17 (O, S, N, P, F, Cl), which are typically used as electron donors in a variety of directional noncovalent interactions.[1,2] They frequently participate in H-bonding,[3] σ,π-hole[4–6] and lp···π interactions[7] that are useful in crystal engineering. More recently, it has been demonstrated that late transition metals centres can act as electron donors in σ-hole interactions.[8,9] For instance, Ni^{II},[10] Rh^{I},[11] Pd^{II},[12,13] Pt^{II},[14,15] and Au^{I},[16–19] are able to behave as halogen,[10–19] chalcogen[20] and pnictogen bond acceptors.[21] A common feature in those interactions is the participation of a lone pair located at the d_{z^2} or $d_{x^2-y^2}$ atomic orbital of the metal centre.

Most recently, it has been described that Pd and Pt metals in planar complexes can act as electron donor centres in π-hole interactions (π-hole···d_{z^2}[M] contacts, M = metal).[22–24] Both metals form square planar complexes that are sterically accessible to interact with π electron-deficient systems. In the field of crystal engineering, two important investigations are worth highlighting. First, the co-crystallization of polyfluoroaromatic species with Pt and Pd complexes (ligands tetraphenylporphyrin, acetylacetone or benzoylacetone) yield reverse arene sandwich structures built by π-hole···[M^{II}] interactions (see Scheme 1).[22] Second, cocrystallization of the palladium acetate cluster $Pd_3(OAc)_6$ with electron-deficient fluoroarenes

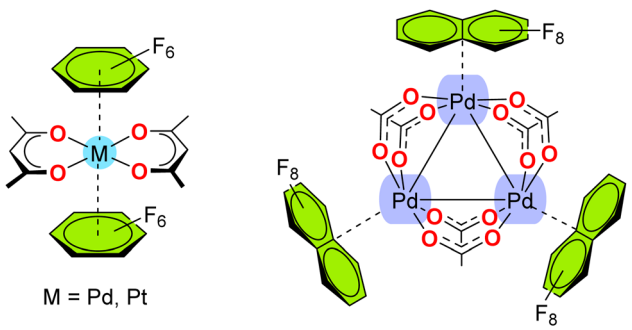

Scheme 1 Left: reverse arene sandwich structure. Right: palladium acetate cluster $Pd_3(OAc)_6$ interacting with three perfluoronaphtalene units.

[a]*NFMLab, Department of Chemistry, Materials, and Chemical Engineering "Giulio Natta", Politecnico di Milano, via L. Mancinelli 7, I-20131 Milano, Italy. E-mail: giuseppe.resnati@polimi.it*
[b]*Departament de Química, Universitat de les Illes Balears, Crta de Valldemossa Km, 7.5, 07122 Palma de mallorca, Baleares, Spain. E-mail: toni.frontera@uib.es*
†Electronic supplementary information (ESI) available. See DOI: https://doi.org/10.1039/d3dt00698k

leads to the formation of inorganic–organic stacking interactions where the electron-rich PdO_4 plane behaves as a five-center nucleophile (combined oxygen lone pairs and the d_{z^2} orbital of Pd) donating electron density to the π-acidic surface of the arenes (see Scheme 1).[25]

Apart from their importance in crystal engineering, π-hole⋯[M^{II}] interactions have been used to enhance the phosphorescence of Pt^{II}-based luminophores.[24] That is, when phosphorescent Pt^{II}-based cyclometalated complexes are co-crystallized with perfluorinated arenes to give 1 : 1 co-crystals, up to 3.5-fold luminescence quantum yield and 15-fold lifetime enhancements are observed. This increase was associated with the strength of the π-hole⋯d_{z^2}[Pt^{II}] contact that is dependent on the π-acidity of the arene.[24]

Apart from Pd and Pt complexes, the π-hole⋯d_{z^2}[M], interaction has been recently demonstrated for Cu(II).[26] This unprecedented example is remarkable, since Cu(II) playing the role of the nucleophile was not demonstrated before. Specifically, cocrystallization of a bis[1-(4-pyridyl)butane-1,3-dionato]copper(II) complex and 1,4-diiodoperfluorobenzene in the presence of pyridine yields a 1 : 1 cocrystal exhibiting π-hole⋯CuO_4 stacking contacts. The {d_{z^2}-$Cu^{II}O_4$} moiety functions as an integrated five-centre π-hole acceptor and the interaction plays a significant structure-guiding role in the solid state of the co-crystal. The nucleophilicity of the Cu(II) atom is due to the square-pyramidal coordination environment and the polarization of the d_{z^2}-orbital due to the presence of an axial pyridine ligand.

In this manuscript, some X-ray structures from the Cambridge Structural Database (CSD) are discussed to evidence how π-hole⋯d_{z^2}[M^{II}] are crucial in determining the X-ray packing. These structures allowed for identifying the molecular entities used for a comprehensive DFT study aimed at an energetic characterization of the interaction and at an analysis of the effect of the metal centre (Ni, Pd, Pt) on the strength of the interaction. Furthermore, the effect of the degree of fluorination of the arene upon the energetic features of the supramolecular complexes has been studied. Finally, it has been demonstrated that the nucleophilicity of the metal centre can be enhanced by the existence of metallophilic interactions at the opposite side, due to the polarization of the d_{z^2}[M^{II}] orbitals.

Methods

CSD analysis

The CSD (Cambridge Structural Database)[27] was interrogated to explore the ability of square planar complexes of Ni, Pd and Pt (number of bonded atoms = 4 was imposed in the search) to interact with six membered aromatic rings. To do so, three intermolecular contacts were defined, between the metal centre and three alternate atoms (1,3,5) of the aromatic ring. Such intramolecular contacts were signalled by interatomic distances less than the sum of van der Waals radii +0.2 Å. Both carbon and nitrogen atoms were used as possible components of the six-membered aromatic rings.

Theoretical methods

The calculations of the non-covalent complexes were carried out using Turbomole 7.2 program[28] and the PBE0[29]-D3[30]/def2-TZVP[31,32] level of theory. For the heavier elements Pd and Pt, this basis set implements ECPs and relativistic effects.[31,32] The complexes were fully optimized using the C_{2v} symmetry constraint. The interaction energies were computed by calculating the difference between the energies of isolated monomers (optimized geometries) and their assembly. In case of the ternary complexes, they were calculated as binary systems, considering the π-stacked M⋯M dimers as monomers. Bader's "atoms in molecules" theory (QTAIM)[33] analysis was performed by means of the Multiwfn program.[34] The molecular electrostatic potential surfaces were visualized using the Gaussview software.[35] In order to investigate the nature of the interactions and reveal them in real space, the NCIplot index was used, which is a method for plotting non-covalent interaction regions[36] based on a visualization index that is derived from the electronic density.[37] The reduced density gradient (RDG), which came from the density and its first derivative, was plotted as a function of the density (mapped as isosurfaces) over the molecule of interest. The sign of the second Hessian eigenvalue times the electron density [*i.e.*, sign(λ_2)ρ in atomic units] enabled the identification of attractive/stabilizing (blue-green coloured isosurfaces) or repulsive (yellow-red coloured isosurfaces) interactions using 3D-plots. The NCIplot index parameters used in this work were: RGD = 0.5; $\rho_{cut\text{-}off}$ = 0.05 a.u.; colour range: −0.035 a.u. ≤ sign(λ_2)ρ ≤ 0.035 a.u. The QTAIM/NCIplot figures were presented using the VMD software.[38]

Results and discussion

CSD exploration

This section discusses a selection of systems from the CSD demonstrating the ability of square planar complexes of Pd and Pt to interact with electron deficient aromatic rings *via* highly directional π-hole⋯d_{z^2}[M^{II}] bondings. In case of Ni, we have not found any example in the CSD, thus suggesting the low nucleophilicity of square planar Ni(II).

Fig. 1 shows four examples where perfluorinated aromatic rings are located parallel to the square planar M(II) complex. RIRMAJ (Fig. 1a) and RIRMEN (Fig. 1b) are 1 : 1 cocrystals of hexafluorobenzene with bis(acetylacetonato)-Pd(II) and bis(acetylacetonato)-Pt(II), respectively.[22] Both form infinite 1D polymeric columns where alternate bis(acetylacetonato)-M(II) and C_6F_6 propagate by means of π-hole⋯d_{z^2}[M^{II}] interactions. A similar 1D infinite assembly is observed in PUNPEW,[24] (Fig. 1c) a 1 : 1 cocrystal of (acetylacetonato)-(2-(1,3-benzothiazol-2-yl)phenyl)-Pt(II) with octafluoronaphthalene. The π-hole⋯d_{z^2}[M^{II}] distances are similar in the three supramolecular polymers (3.228 to 3.313 Å). A discrete trimeric assembly is shown in Fig. 1d, where the (5,10,15,20-tetraphenylporphyrinato)-Pt(II) interacts with two hexafluorobenzene molecules above and below the porphyrinato plane. The π-hole⋯d_{z^2}[M^{II}]

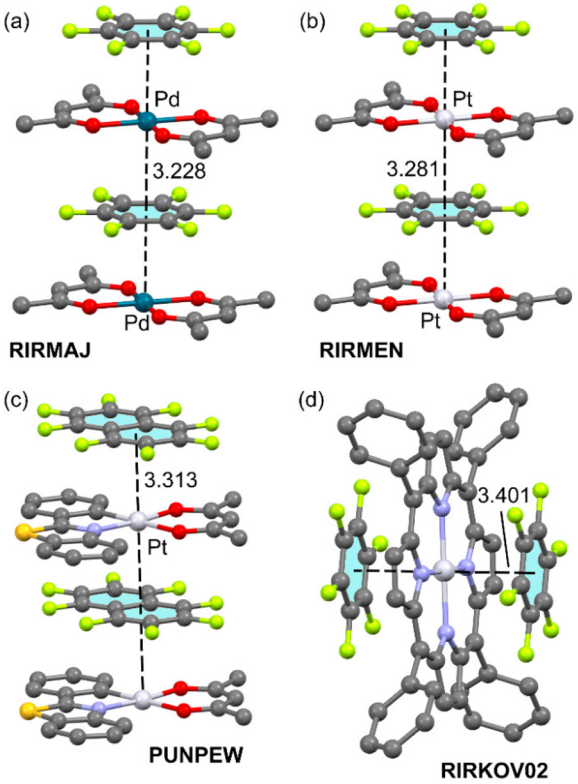

Fig. 1 Partial views of the X-ray structures of CSD codes RIRMAJ (a), RIRMEN (b), PUNPEW (c) and RIRKOV (d). Distances in Å calculated from the metal to the ring centroid apart from PUNPEW where it is measured to the ring plane. H-atoms omitted for clarity. Colour code: fluorine lime, oxygen red, nitrogen blue, sulfur yellow, palladium teal and platinum grey.

distances are longer (3.401 Å) in this assembly likely due to the lower nucleophilicity of the PtN_4 core with respect to the PtO_4 (RIRMEN) or $PtCNO_2$ (PUNPEW) cores.

Two interesting examples involving a common palladium acetate cluster $Pd_3(OAc)_6$ are shown in Fig. 2.[25] Both systems show structure-directing inorganic–organic stacking interactions. In these stacking interactions, the electron-rich PdO_4 unit behaves as a five-center nucleophile providing oxygen lone pairs in addition to the d_{z^2}-Pd(II) orbital to effectively complement the π-acidic surface of the arenes. The CAPBAA[25] structure (Fig. 2a) is a 1 : 2 cocrystal where two 1,2-di-iodotetrafluorobenzene rings interact with two PdO_4 units of the metallic cluster with distances that are similar to those of the infinite assemblies of Fig. 1. Interestingly, in CANZOK (Fig. 2b)[25] three octafluoronaphthalene rings interact with the three PdO_4 units of the metallic cluster, thus completely wrapping the inorganic part of the co-crystal by means of π-hole$\cdots d_{z^2}[M^{II}]$ interactions.

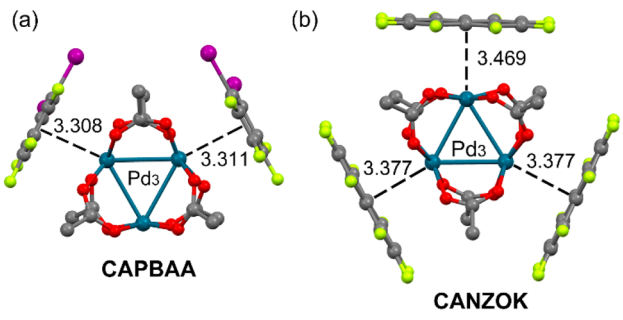

Fig. 2 Partial views of the X-ray structures of CSD codes CAPBAA (a) and CANZOK (b). Distances in Å calculated from the metal to the ring centroid in (a) to the ring plane in (b). H-atoms omitted for clarity. Colour code: fluorine lime, oxygen red, iodine purple, palladium teal.

A remarkable self-assembly is represented in Fig. 3a, where a supramolecular dimer of an acetylacetonate Pt(II) complex with an azabuckybowl co-ligand is represented (DAWQUR).[39] It can be observed that the Pt-atom is located over the centre of the central six-membered ring of the azahomosumanene fragment at a distance that is similar to those observed for the interaction of Pt with the perfluorinated rings (Fig. 1 and 2). The MEP surface of the monomer is represented in Fig. 3b, evidencing the nucleophilicity of the Pt-atom (−29 kcal mol^{-1}), in fact it corresponds to the MEP minimum. Most importantly, the MEP is positive only over the centre of the central six-membered ring and it is negative over the rest of six membered rings. This strongly suggests the π-hole$\cdots d_{z^2}[M^{II}]$ nature of the

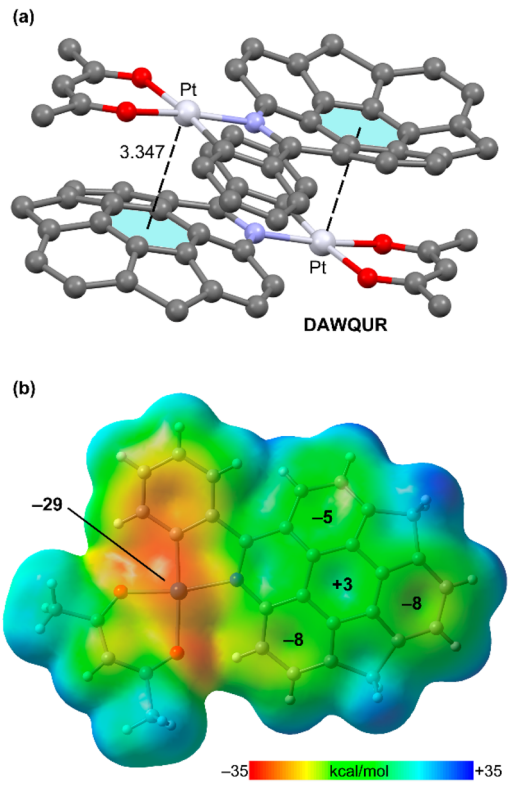

Fig. 3 (a) Partial views of the X-ray structures of CSD code DAWQUR. Distance in Å calculated from the metal to the ring centroid. H-atoms omitted for clarity. Colour code: oxygen red, nitrogen blue and platinum grey. (b) MEP surface of DAWQUR at the PBE0-D3/def2-TZVP level of theory. The values are given in kcal mol^{-1}. Density isosurface 0.002 a.u.

interaction and that this interaction is, in fact, governing the crystal packing of DAWQUR.

Other examples of π-hole···$d_{z^2}[M^{II}]$ interactions involving non-fluorinated rings are given in Fig. 4. The first one (JITYEQ[40]) corresponds to a salt formed by 4,4′-bipyridinium dication tetrachloro-Pt(II) dianion. In the solid state (Fig. 4a), each tetrachloro-Pt(II) dianion interacts with two pyridinium rings one above and one below the molecular plane at 3.450 Å from the ring centres. This distance is comparable to those observed for the structures commented above. The other selected example (SERDOJ,[41] Fig. 4b) is a neutral dichloro-(6,7-dicyanodipyridoquinoxaline)-Pt(II) complex [$PtLCl_2$]. It is worthy to highlight that in the solid state it forms extended π-hole···$d_{z^2}[Pt^{II}]$/$[Pt^{II}]$···$[Pt^{II}]$/π-hole···$d_{z^2}[Pt^{II}]$ networks. That is, self-assembled dimers with an antiparallel orientation of the [$PtLCl_2$] units and two symmetrically equivalent π-hole···$d_{z^2}[Pt^{II}]$ interactions (3.418 Å) are connected *via* metallophilic Pt···Pt contacts (3.358 Å). The theoretical section below shows that this metallophilic contacts increase the nucleophilicity of the Pt-atoms.

Finally, it is worthy to comment the X-ray structure of reference code VOLKAK[42] where a Pt(II) square planar complex interacts with an electron rich aromatic ring (Fig. 5). This example is a benzene solvate where the Pd(II) metal centre is coordinated to two bis(pentafluorobenzoyl)methanido ligands. In the crystal structure, two solvent molecules are located above and below the PdO_4 plane (Fig. 5a) with asymmetric distances (3.414 Å and 3.357 Å). It has been demonstrated that two forces are important to rationalize ion–π interactions. One is the electrostatic term that basically depends on the sign of the quadrupole moment of the arene, and the other one is the polarization term that depends on the induced dipole due to the approach of the anion/cation to the π-system.[43,44]

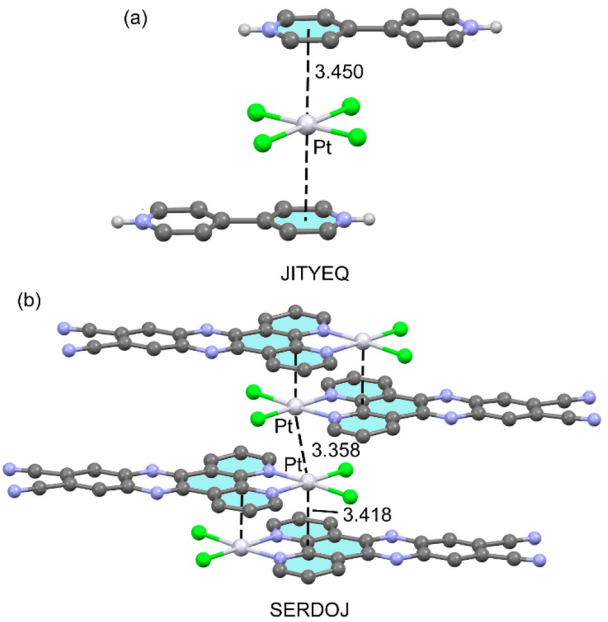

Fig. 4 Partial views of the X-ray structures of CSD codes JITYEQ (a) and SERDOJ (b). Distances in Å calculated from the metal to the ring centroid in (a) and to the ring plane in (b). H-atoms omitted for clarity apart from those bonded to pyridine N-atoms in (a). Colour code: chlorine green, nitrogen blue, platinum light grey.

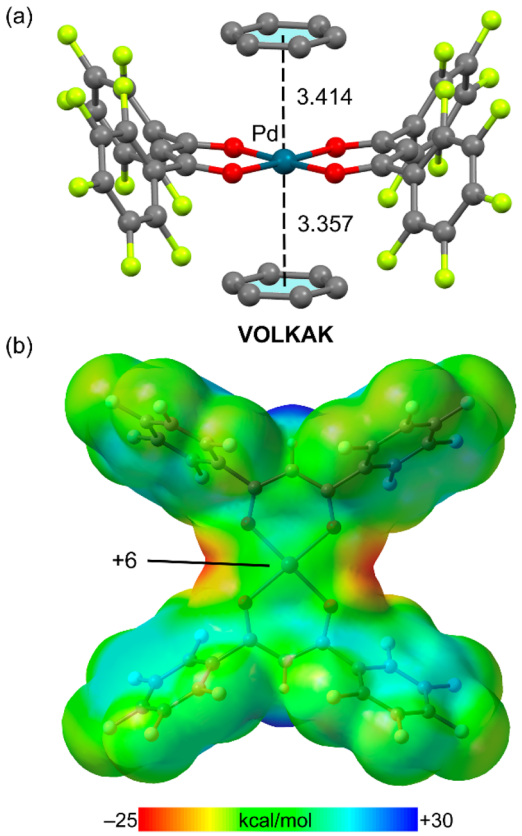

Fig. 5 (a) Partial views of the X-ray structures of CSD code VOLKAK. Distance in Å calculated from the metal to the ring centroid. H-atoms omitted for clarity. Colour code: oxygen red, fluorine lime and palladium teal. (b) MEP surface of VOLKAK at the PBE0-D3/def2-TZVP level of theory. The values are given in kcal mol^{-1}. Density isosurface 0.002 a.u.

The molecular electrostatic potential (MEP) surface of the Pd(II) complex is shown in Fig. 5b, showing that in this case the MEP at the Pd-atom is slightly positive, thus suggesting a small electrostatic attraction between the negative component of the quadrupole moment of benzene (parallel to the C_6 axis) and the metal centre. The lack of nucleophilicity of the Pd complex in VOLKAK is likely due to the electron withdrawing effect of the four pentafluorobenzene rings of the ligands that reduces the charge density at the Pd(II) atom.

DFT study of model systems

A theoretical analysis has been performed on some model systems inspired by the structures discussed above to investigate the energetic features of the arene···$[M^{II}]$ interactions and the influence of the arene, the group-10 element, and the presence of metallophilic interactions at the opposite side, as detailed in the following sections.

MEP analysis

The MEP surface analysis of the model compounds **1–10** (Scheme 2) was carried out in order to investigate the nucleophilic/electrophilic character of the arenes **1–4** and the nucleophilic character of the square planar complexes **5–7** and their supramolecular dimers (**8–10**). The surfaces are represented in Fig. 6 and the MEP values gathered in Table 1. The MEP values over the centre of the arene ($V_{s,Cg}$) become more positive on going from **1** to **4**, being negative for **1** and **2** and positive for **3** and **4**. Regarding the metal complexes, the nucleophilicity increases when going down in the group, as previously demonstrated.[9] Interestingly, the nucleophilicity of the metal centre increases (1–3 kcal mol^{-1}) in the supramolecular dimers **8–10** with respect to the monomers **5–7**. In fact, the MEP value at the Pt-atom in **10** (−17.6 kcal mol^{-1}) is comparable to that of benzene.

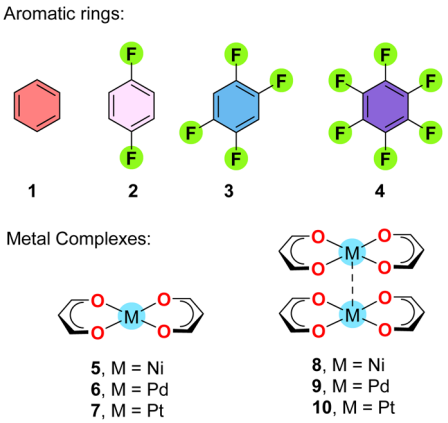

Scheme 2 Aromatic rings **1–4** and metal complexes **5–10** used in this work.

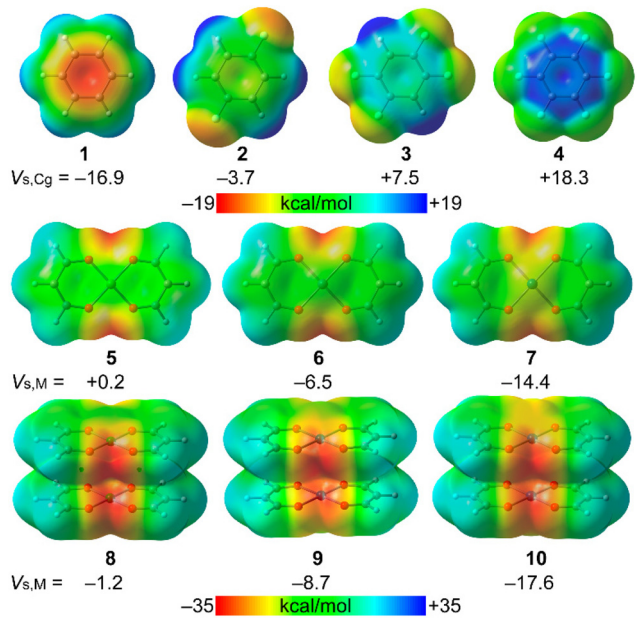

Fig. 6 MEP surfaces of compounds **1–10** at the PBE0-D3/def2-TZVP level of theory. The values over the ring centroid ($V_{s,Cg}$) or over the metal center ($V_{s,M}$) are given in kcal mol^{-1}.

Table 1 MEP values over the ring centroid and over the metal centre in compounds **1–10**

Compound	$V_{s,min}$	$V_{s,max}$	$V_{s,Cg}$ or $V_{s,M}$
1	−16.9	+14.4	−16.9
2	−12.7	+21.4	−3.7
3	−11.1	+29.6	+7.5
4	−5.1	+18.3	+18.3
5	−37.4	+19.1	+0.2
6	−35.9	+19.9	−6.5
7	−34.0	+20.5	−14.4
8	−41.9	+19.1	−1.2
9	−40.4	+19.8	−8.7
10	−38.6	+20.2	−17.6

Energetic study

Table 2 shows the interaction energies and equilibrium distances of complexes **11–22** (Scheme 3), where two different orientations of the benzene ring have been analysed. The differences between both orientations in terms of binding energies and equilibrium distances are modest (up to 0.9 kcal mol^{-1}) thus suggesting that the aromatic ring can adopt any orientation over the complex if parallel to the metal complex.

All complexes exhibit favourable interaction energies ranging from −5.91 kcal mol^{-1} in **15b** to −10.26 kcal mol^{-1} in **22b**. The fact that even the most nucleophilic Pt(II) complexes form stable complexes with benzene (electron rich π-system) confirms that, in this type of binding, polarization/induction effects are important and, consequently, the interaction cannot be rationalized only in terms of electrostatic effects. Nevertheless, the most favourable complex corresponds to **22b**, where the most nucleophilic Pt(II) complex interacts with the most electron deficient aromatic ring (hexafluorobenzene) in line with the MEP analysis. Moreover, for all metal complexes, the interaction energies become more favourable (negative) on going from benzene to hexafluorobenzene, in line with the expected π-hole$\cdots$d$_{z^2}$[M^{II}] nature of the dimers. In Table 2 the contribution of the dispersion correction is indicated. The values given in Table 2 have been simply estimated using the D3 dispersion correction instead of using a partition energy analysis. It is well known that dispersion is needed to properly describe π-stacking assemblies using DFT methods.[30] This is also the case in this type of bonding where the aromatic ring is stacked over the square planar complex. Actually, the dispersion contribution values gathered in Table 2 are larger (or very close) than the interaction energies for the assemblies involving the electron rich arenes **1** and **2** and smaller for electron poor arenes **3** and **4**. This evidences that dispersion gives a major contribution and that the electrostatic repulsion/attraction is smaller when compared to the dispersion. The fact that the dispersion contribution is larger than the interaction energies for the assemblies with the electron rich arenes agrees well with the MEP analysis, where the electro-

Table 2 Interaction energies (E, kcal mol^{-1}), D3 dispersion contribution (E_{disp}. kcal mol^{-1}) and equilibrium distances (d, Å) from the metal to the ring centroid for complexes **11–22**

Complex	E	E_{disp}	d
11a (**1** + **5**)	−6.05	−6.57	3.377
11b (**1** + **5**)	−6.06	−6.69	3.360
12a (**2** + **5**)	−6.58	−6.48	3.405
12b (**2** + **5**)	−6.39	−6.78	3.358
13a (**3** + **5**)	−8.23	−7.39	3.294
13b (**3** + **5**)	−8.80	−7.33	3.315
14a (**4** + **5**)	−8.81	−7.11	3.317
14b (**4** + **5**)	−9.40	−7.50	3.292
15a (**1** + **6**)	−5.92	−6.45	3.423
15b (**1** + **6**)	−5.91	−6.50	3.432
16a (**2** + **6**)	−6.68	−6.31	3.490
16b (**2** + **6**)	−6.27	−6.71	3.418
17a (**3** + **6**)	−8.05	−7.30	3.365
17b (**3** + **6**)	−8.83	−7.35	3.376
18a (**4** + **6**)	−8.92	−7.17	3.382
18b (**4** + **6**)	−9.55	−7.60	3.354
19a (**1** + **7**)	−6.13	−7.69	3.411
19b (**1** + **7**)	−6.12	−7.72	3.407
20a (**2** + **7**)	−7.13	−7.63	3.438
20b (**2** + **7**)	−6.62	−7.96	3.399
21a (**3** + **7**)	−8.52	−8.55	3.357
21b (**3** + **7**)	−9.42	−8.58	3.362
22a (**4** + **7**)	−9.69	−8.45	3.378
22b (**4** + **7**)	−10.26	−8.85	3.351

Two orientations for the complexes:

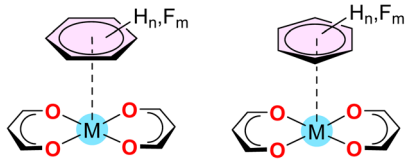

11a, M = Ni, n = 6, m = 0 **11b**, M = Ni, n = 6, m = 0
12a, M = Ni, n = 4, m = 2 **12b**, M = Ni, n = 4, m = 2
13a, M = Ni, n = 2, m = 4 **13b**, M = Ni, n = 2, m = 4
14a, M = Ni, n = 0, m = 6 **14b**, M = Ni, n = 0, m = 6
15a, M = Pd, n = 6, m = 0 **15b**, M = Pd, n = 6, m = 0
16a, M = Pd, n = 4, m = 2 **16b**, M = Pd, n = 4, m = 2
17a, M = Pd, n = 2, m = 4 **17b**, M = Pd, n = 2, m = 4
18a, M = Pd, n = 0, m = 6 **17b**, M = Pd, n = 0, m = 6
19a, M = Pt, n = 6, m = 0 **19b**, M = Pt, n = 6, m = 0
20a, M = Pt, n = 4, m = 2 **20b**, M = Pt, n = 4, m = 2
21a, M = Pt, n = 2, m = 4 **21b**, M = Pt, n = 2, m = 4
22a, M = Pt, n = 0, m = 6 **22b**, M = Pt, n = 0, m = 6

Scheme 3 Supramolecular complexes **11–22** studied in this work. The difluoro and tetrafluoro aromatic rings were oriented in such a way to have C_{2v} symmetry.

static repulsion is largely compensated by the dispersion. The opposite occurs for the electron poor arenes, where the binding energies are larger than dispersion contribution, evidencing a favourable electrostatic contribution. An interesting result is that the dispersion contribution increases when going down in the group-10 of elements, thus explaining the slightly larger interaction energy of the Pt(II) complex with benzene (**19**) than Ni(II) or Pd(II) complexes (**11** and **15**, respectively). Finally, the variation in interaction energies on going from Ni to Pt are not very significant. For instance, for the complexes with hexafluorobenzene **4**, series "b", the energies are −8.80 kcal mol^{-1} for Ni, −9.55 kcal mol^{-1} for Pd and −10.26 kcal mol^{-1} for Pt. Remarkably, the equilibrium distances summarized in Table 2 range from 3.292 Å (**14b**) to 3.490 Å (**16a**), namely separations are very similar to those found in the X-ray structures and gives reliability to the level of theory.

As mentioned above, we have also analysed the effect of the metallophilic contact upon the strength of the π···[M^{II}] interaction at the opposite side.

To do so, we have computed the complexes indicated in Scheme 4 and compared the interaction energies and equilibrium distances of the trimeric assemblies (Table 3) with those of the dimeric assemblies (Table 2).

It can be observed that indeed the interaction energies are slightly more negative for complexes **23–34** than those of **11–22** suggesting a favourable cooperativity between the two interactions. The reinforcement of the interaction is very small (<1 kcal mol^{-1}) in line with the small variation of the MEP values in compounds **8–10** compared to those of dimers **5–7**. Also it is interesting that the dispersion contribution increases in the ternary assemblies with respect to the binary ones, thus suggesting that dispersion effects are also relevant reinforcing the π···M interactions.

QTAIM/NCIPlot analysis

In order to characterize the π···M interactions in the complexes **11** to **34**, we have used a combination of QTAIM and NCIplot computational tools. They are useful to visualize interactions in real space. The QTAIM/NCIplot analyses of the platinum binary and "a" series ternary complexes are given in Fig. 7 and 8, respectively. The rest of complexes are given in the ESI (Fig. S1–S5†).

Two orientations for the complexes:

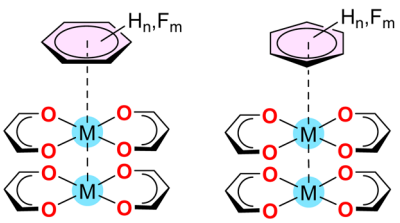

23a, M = Ni, n = 6, m = 0 **23b**, M = Ni, n = 6, m = 0
24a, M = Ni, n = 4, m = 2 **24b**, M = Ni, n = 4, m = 2
25a, M = Ni, n = 2, m = 4 **25b**, M = Ni, n = 2, m = 4
26a, M = Ni, n = 0, m = 6 **26b**, M = Ni, n = 0, m = 6
27a, M = Pd, n = 6, m = 0 **27b**, M = Pd, n = 6, m = 0
28a, M = Pd, n = 4, m = 2 **28b**, M = Pd, n = 4, m = 2
29a, M = Pd, n = 2, m = 4 **29b**, M = Pd, n = 2, m = 4
30a, M = Pd, n = 0, m = 6 **30b**, M = Pd, n = 0, m = 6
31a, M = Pt, n = 6, m = 0 **31b**, M = Pt, n = 6, m = 0
32a, M = Pt, n = 4, m = 2 **32b**, M = Pt, n = 4, m = 2
33a, M = Pt, n = 2, m = 4 **33b**, M = Pt, n = 2, m = 4
34a, M = Pt, n = 0, m = 6 **34b**, M = Pt, n = 0, m = 6

Scheme 4 Supramolecular complexes **23–34** studied in this work. The difluoro and tetrafluoro aromatic rings were oriented in such a way to have C_{2v} symmetry.

Table 3 Interaction energies (E, kcal mol^{-1}), dispersion contribution (E_{disp}. kcal mol^{-1}), equilibrium distances (d, Å) from the metal to the ring for complexes **23–34**

Complex	E	E_{disp}	d
23a (**1** + **8**)	−6.22	−6.94	3.383
23b (**1** + **8**)	−6.21	−6.74	3.395
24a (**2** + **8**)	−6.75	−6.76	3.418
24b (**2** + **8**)	−6.60	−7.18	3.372
25a (**3** + **8**)	−8.59	−7.79	3.303
25b (**3** + **8**)	−9.10	−7.68	3.325
26a (**4** + **8**)	−9.14	−7.46	3.337
26b (**4** + **8**)	−9.82	−7.85	3.298
27a (**1** + **9**)	−6.11	−6.94	3.446
27b (**1** + **9**)	−6.12	−6.96	3.444
28a (**2** + **9**)	−6.88	−6.91	3.470
28b (**2** + **9**)	−6.56	−7.23	3.429
29a (**3** + **9**)	−8.50	−7.92	3.376
29b (**3** + **9**)	−9.21	−7.88	3.393
30a (**4** + **9**)	−9.35	−7.65	3.403
30b (**4** + **9**)	−10.00	−8.00	3.370
31a (**1** + **10**)	−6.30	−8.22	3.416
31b (**1** + **10**)	−6.17	−8.10	3.399
32a (**2** + **10**)	−7.37	−8.21	3.446
32b (**2** + **10**)	−6.93	−8.45	3.400
33a (**3** + **10**)	−9.04	−9.22	3.357
33b (**3** + **10**)	−9.89	−9.25	3.373
34a (**4** + **10**)	−10.25	−9.09	3.383
34b (**4** + **10**)	−10.86	−9.52	3.354

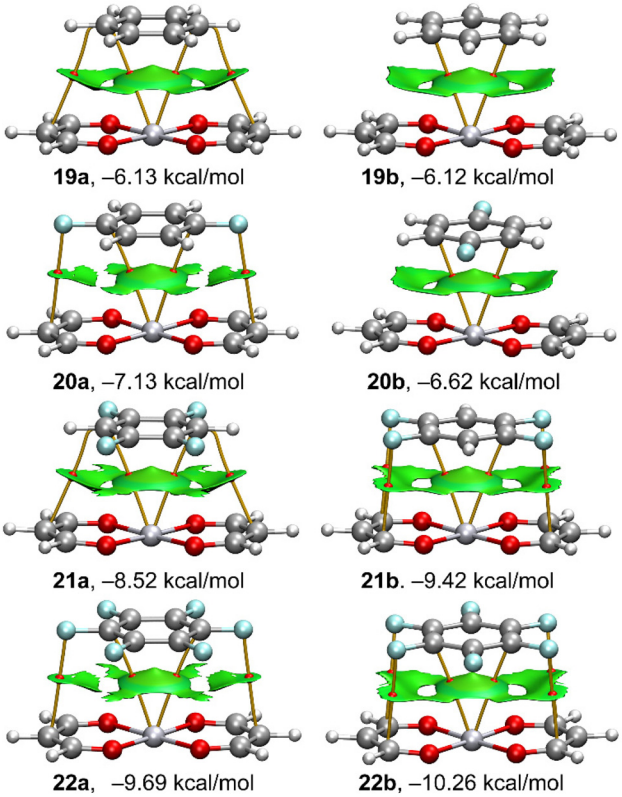

Fig. 7 QTAIM (bond CPs in red and bond paths as solid lines) and NCIPlot (RDG = 0.5 a.u., ρ cut-off = 0.05 a.u., colour range ±0.035 a.u.) for platinum complexes **19–22**.

For the binary assemblies (Fig. 7), it can be observed that in all cases the Pt atom is connected to the aromatic ring through two bond critical points (CPs, represented as red spheres) and bond paths. In some complexes, additional bond CPs and bond paths interconnect both monomers, disclosing the existence of supplementary F···C (**20a**, **21b** and **22a**,**b**) or C···C (**19a**, **21a**) contacts. It is worth mentioning that the O-atoms of the PtO_4 core are not connected to the aromatic rings, thus suggesting the main role of the metal centre in the binding mechanism.

This is also observed for the rest of complexes (Fig. S1–S5†). From the NCIplot analysis, it can be observed a large and extended isosurface that embraces the whole arene, as it is typical in π-stacking interactions. The surface also reaches the region of the H/F-atoms, thus suggesting a strong complementarity of the systems and a large van der Waals contact region. This also agrees with the fact that all interaction energies are favourable with the large contribution of dispersion forces.

For the ternary assemblies (Fig. 8), we discuss here the Pt (II)-complexes in the "a" orientation. The rest of complexes are given in the ESI (see Fig. S3–S5†). Regarding the π···M interaction, the distribution of bond CPs, bond paths and reduced density gradient (RDG) isosurfaces is identical to those of the binary complexes. Regarding the Pt···Pt interaction, it is characterized by a bond CP, bond path and disk shaped RDG isosurface. The PtL_2···PtL_2 stacking is further characterized by two symmetrically equivalent bond CPs and bond paths interconnecting two carbon atoms of the ligands. The shape of the RDG isosurface that is located between the organic ligands indicates some contribution from the π-staking of the conjugated π-systems of the ligands.

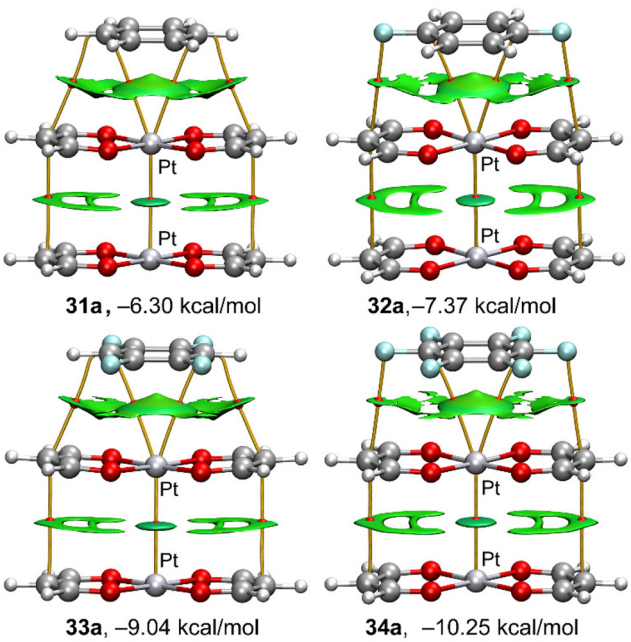

Fig. 8 QTAIM (bond CPs in red and bond paths as solid lines) and NCIPlot (RDG = 0.5 a.u., ρ cut-off = 0.05 a.u., colour range ±0.035 a.u.) for platinum complexes **31a–34a**.

Conclusions

In this work, the structure-directing role of π-hole···d_{z^2}[M^{II}] interactions has been evidenced using theoretical calculations on model systems identified *via* an analysis of CSD structures displaying the mentioned interaction. Four different arenes and three square planar complexes were considered. The investigated interactions have been recently used in crystal engineering to generate unprecedented solid state architectures. However, a comprehensive theoretical analysis and a critical discussion of X-ray structures was not accessible. Some relevant conclusions derived from this work are as follows: (1) square planar complexes of Ni, Pd and Pt have the ability to interact favourably with arenes, independently of the electronic nature of the arene (electron deficient or electron rich), though the binding energies are stronger with the electron deficient ones; (2) if the arene plane remains orthogonal to the d_{z^2} orbital, the orientation of the latter has modest influence on the binding energies of the complex; (3) the interaction energies range from −5.91 kcal mol^{-1} to −10.26 kcal mol^{-1}, being the platinum complexes the most favoured; (4) the combined QTAIM analysis suggests that it is basically the metal centre that interacts with the arene, rather than the O-atoms directly bonded to the metal centre; (5) the NCIplot evidences a high complementarity between the planar systems and a large van der Waals contact region; (6) the existence of a metallophilic M···M interaction opposite to the π-hole···d_{z^2}[M^{II}] interaction marginally strengthens the π···M interaction.

Attractive interactions of metals with the electron deficient arenes are, to now, poorly explored but it is expected that they will be more and more exploited in the future. The here described understanding of some basic features of these interactions may be instrumental in their fruitful use in crystal engineering and inorganic supramolecular chemistry.

Author contributions

A. F. and G. R. conceived the project. M. C. and S. B. performed the calculations. A. F. and G. R. analysed the data. A. F. and G. R. wrote the paper. A. F. and G. R. supervised the project. A. F. and G. R. were responsible for funding acquisition.

Conflicts of interest

There are no conflicts to declare.

Acknowledgements

This research was partially funded by the "Ministerio de Ciencia, Investigacion y Universidades/Agencia Estatal de Investigación" (MICIU/AEI/10.13039/501100011033) of Spain (project PID2020-115637GB-I00. FEDER funds). We thank the Centre de Tecnologies de la Informació (CTI) at University of the Balearic Islands (UIB) for the technical support.

References

1 I. Alkorta, J. Elguero and A. Frontera, *Crystals*, 2020, **10**, 180.
2 A. Frontera and A. Bauzá, *Crystals*, 2021, **11**, 1205.
3 S. J. Grabowski, *J. Phys. Org. Chem.*, 2004, **17**, 18–31.
4 L. C. Gilday, S. W. Robinson, T. A. Barendt, M. J. Langton, B. R. Mullaney and P. D. Beer, *Chem. Rev.*, 2015, **115**, 7118–7195.
5 G. Cavallo, P. Metrangolo, R. Milani, T. Pilati, A. Priimagi, G. Resnati and G. Terraneo, *Chem. Rev.*, 2016, **116**, 2478–2601.
6 A. Bauzá, T. J. Mooibroek and A. Frontera, *ChemPhysChem*, 2015, **16**, 2496–2517.
7 T. J. Mooibroek, P. Gamez and J. Reedijk, *CrystEngComm*, 2008, **10**, 1501–1515.
8 D. M. Ivanov, N. A. Bokach, V. Yu. Kukushkin and A. Frontera, *Chem. – Eur. J.*, 2022, **28**, e202103173.
9 I. Benito, R. M. Gomila and A. Frontera, *CrystEngComm*, 2022, **24**, 4440–4446.
10 Z. M. Bikbaeva, D. M. Ivanov, A. S. Novikov, I. V. Ananyev, N. A. Bokach and V. Y. Kukushkin, *Inorg. Chem.*, 2017, **56**, 13562–13578.
11 D. W. Shaffer, S. A. Ryken, R. A. Zarkesh and A. F. Heyduk, *Inorg. Chem.*, 2012, **51**, 12122–12131.
12 Y. Yamashina, Y. Kataoka and Y. Ura, *Eur. J. Inorg. Chem.*, 2014, 4073–4078.
13 S. V. Baykov, U. Dabranskaya, D. M. Ivanov, A. S. Novikov and V. P. Boyarskiy, *Cryst. Growth Des.*, 2018, **18**, 5973–5980.
14 R. A. Gossage, A. D. Ryabov, A. L. Spek, D. J. Stufkens, J. A. M. van Beek, R. van Eldik and G. van Koten, *J. Am. Chem. Soc.*, 1999, **121**, 2488–2497.
15 D. M. Ivanov, A. S. Novikov, I. V. Ananyev, Y. V. Kirina and V. Y. Kukushkin, *Chem. Commun.*, 2016, **52**, 5565–5568.
16 H. M. Yamamoto, J.-I. Yamaura and R. Kato, *J. Am. Chem. Soc.*, 1998, **120**, 5905–5913.
17 R.-Y. Liau, H. Ehlich, A. Schier and H. Schmidbaur, *Z. Naturforsch., B: J. Chem. Sci.*, 2002, **57**, 1085.
18 A. S. Novikov, *Inorg. Chim. Acta*, 2018, **471**, 126–129.
19 L. Andreo, R. M. Gomila, E. Priola, A. Giordana, S. Pantaleone, E. Diana, G. Mahmoudi and A. Frontera, *Cryst. Growth Des.*, 2022, **22**, 6539–6544.
20 A. V. Rozhkov, E. A. Katlenok, M. V. Zhmykhova, A. Yu. Ivanov, M. L. Kuznetsov, N. A. Bokach and V. Yu. Kukushkin, *J. Am. Chem. Soc.*, 2021, **143**, 15701–15710.
21 S. Burguera, R. M. Gomila, A. Bauzá and A. Frontera, *Inorganics*, 2023, **11**, 80.
22 A. V. Rozhkov, M. A. Krykova, D. M. Ivanov, A. S. Novikov, A. A. Sinelshchikova, M. V. Volostnykh, M. A. Konovalov,

M. S. Grigoriev, Y. G. Gorbunova and V. Y. Kukushkin, *Angew. Chem., Int. Ed.*, 2019, **58**, 4164–4168.
23 S. V. Baykov, S. I. Filimonov, A. V. Rozhkov, A. S. Novikov, I. V. Ananyev, D. M. Ivanov and V. Y. Kukushkin, *Cryst. Growth Des.*, 2020, **20**, 995–1008.
24 A. V. Rozhkov, I. V. Ananyev, R. M. Gomila, A. Frontera and V. Y. Kukushkin, *Inorg. Chem.*, 2020, **59**, 9308–9314.
25 Y. V. Torubaev, I. V. Skabitsky, A. V. Rozhkov, B. Galmés, A. Frontera and V. Yu. Kukushkin, *Inorg. Chem. Front.*, 2021, **8**, 4965–4975.
26 D. Blasi, V. Nicolai, R. M. Gomila, P. Mercandelli, A. Frontera and L. Carlucci, *Chem. Commun.*, 2022, **58**, 9524–9527.
27 C. R. Groom, I. J. Bruno, M. P. Lightfoot and S. C. Ward, *Acta Crystallogr., Sect. B: Struct. Sci., Cryst. Eng. Mater.*, 2016, **72**, 171–179.
28 R. Ahlrichs, M. Bär, M. Häser, H. Hom and C. Kölmel, *Chem. Phys. Lett.*, 1989, **162**, 165–169.
29 C. Adamo and V. Barone, *J. Chem. Phys.*, 1999, **110**, 6158–6169.
30 S. Grimme, J. Antony, S. Ehrlich and H. Krieg, *J. Chem. Phys.*, 2010, **132**, 154104.
31 F. Weigend, *Phys. Chem. Chem. Phys.*, 2006, **8**, 1057–1065.
32 F. Weigend and R. Ahlrichs, *Phys. Chem. Chem. Phys.*, 2005, **7**, 3297–3305.
33 R. F. W. Bader, *J. Phys. Chem. A*, 1998, **102**, 7314–7323.
34 T. Lu and F. Chen, *J. Comput. Chem.*, 2012, **33**, 580–592.
35 R. Dennington, T. A. Keith and J. M. Millam, *GaussView, Version 6.1*, Semichem Inc., Shawnee Mission, KS, 2016.
36 J. Contreras-García, E. R. Johnson, S. Keinan, R. Chaudret, J.-P. Piquemal, D. N. Beratan and W. Yang, *J. Chem. Theory Comput.*, 2011, **7**, 625–632.
37 E. R. Johnson, S. Keinan, P. Mori-Sánchez, J. Contreras-García, A. J. Cohen and W. Yang, *J. Am. Chem. Soc.*, 2010, **132**, 6498–6506.
38 W. Humphrey, A. Dalke and K. Schulten, *J. Mol. Graphics*, 1996, **14**, 33–38.
39 M. Nishimoto, Y. Uetake, Y. Yakiyama, F. Ishiwari, A. Saeki and H. Sakurai, *J. Org. Chem.*, 2022, **87**, 2508–2519.
40 G. R. Lewis and A. G. Orpen, *Chem. Commun.*, 1998, 1873–1874.
41 S. Delahaye, C. Loosli, S.-X. Liu, S. Decurtins, G. Labat, A. Neels, A. Loosli, T. Ward and A. Hauser, *Adv. Funct. Mater.*, 2006, **16**, 286–295.
42 K. Nakajima and A. Hori, *Cryst. Growth Des.*, 2014, **14**, 3169–3173.
43 A. Frontera, P. Gamez, M. Mascal, T. J. Mooibroek and J. Reedijk, *Angew. Chem., Int. Ed.*, 2011, **50**, 9564–9583.
44 C. Garau, D. Quiñonero, A. Frontera, P. Ballester, A. Costa and P. M. Deyà, *Org. Lett.*, 2003, **5**, 2227–2229.